Numerical MPM Solution of Sea Ice Dynamics with an Elastic-Decohesive Constitutive Model

K. Peterson[a], *D. Sulsky*[a,b] *and H. Schreyer*[b]
[a]Department of Mathematics and Statistics
[b]Department of Mechanical Engineering
University of New Mexico
Albuquerque, NM, USA

ABSTRACT

A numerical technique called the material-point method (MPM) shows promise for treating problems of ice dynamics. MPM is based on particle-in-cell technology and thus uses a Lagrangian set of material points with associated mass, position, velocity, stress, and other material parameters, and a background mesh where the momentum equation is solved. This method avoids the convection errors associated with fully Eulerian methods as well as the mesh entanglement that can occur with fully Lagrangian methods under large deformations. Example calculations are performed for a rectangular region of Arctic ice using a newly-developed elastic-decohesive constitutive model. In the simulations, the ice motion is wind-driven and resisted by ocean drag. Two adjacent sides of the rectangle are rigid shorelines and the other two edges are free surfaces that can deform freely. These MPM calculations are compared with published finite element simulations using a viscous-plastic rheology.

KEY WORDS: Sea Ice; Material-Point Method; Elastic-Decohesion

INTRODUCTION

The pack ice is effected by both thermodynamic and mechanical processes. Thermodynamic processes result in mass changes at the atmosphere and ocean boundaries. Mechanical processes can result in the formation of leads and pressure ridges, for example. Motion of the ice pack is driven by the atmosphere and ocean. The ice pack is able to move and deform because of concentrated deformations at leads. Leads form and new areas of open water are exposed. When the driving forces cause the ice to converge, convergence is accommodated by closing open water, and, if necessary, rearranging thin ice by rafting or ridging. An elastic-decohesive constitutive model for pack ice has been developed that explictly accounts for leads (Schreyer et al., 2006). The constitutive model is based on elasticity combined with a cohesive crack law that predicts the initiation, orientation and opening of leads, and also has a simple closing model. Several features were designed into the model. First, the model was constructed to transition from observed brittle failure under tension, to compressive brittle failure under moderate compression, and to a plastic-like faulting under large confinement (Schulson, 2004). The various modes of failure occur in the model, depending on the stress state in the ice. Where the transitions occur in stress space depends on the material parameters and can be adjusted based on empirical data. Second, the model can handle multiple cracks at a point, and therefore can predict crack branching. Third, the numerical implementation of the model is accomplished similarly to standard plasticity models. Thus, in principle, modular codes that call a subroutine to implement the constitutive model can substitute the elastic-decohesion model if it proves worthwhile.

Numerical solutions of mechanics problems where cracks are explicitly included are notoriously difficult to obtain robustly. A numerical technique called the material-point method (MPM) shows promise for treating this class of problems (Sulsky et al., 1995, 2005). MPM is based on particle-in-cell technology and thus uses a Lagrangian set of material points with associated mass, position, velocity, stress, and other material parameters, and a background mesh where the momentum equation is solved. This method avoids the convection errors associated with fully Eulerian methods as well as the mesh entanglement that can occur with fully Lagrangian methods under large deformations. Moreover, the material points are not connected to one another except through the solution of the momentum equation. Thus, as a lead forms, the points can separate without having to alter data structures as would be necessary in standard finite element methods. To demonstrate the elastic-decohesive constitutive model using MPM, simple calculations are performed for rectangular regions of Arctic ice. The calculations are wind-driven and include

ocean drag. These calculations are modeled after similar studies in Schulkes et al. (1998) where more standard viscous and viscous-plastic models for sea ice rheology are compared.

This paper is organized as follows. First, the governing equations used to model sea ice dynamics are specified. Next, the elastic-decohesive constitutive model for sea ice is described. The following section discusses the numerical solution technique. Calculations are presented after this description of the method, followed by a discussion of the results. Finally concluding comments are made.

GOVERNING EQUATIONS

The motion of sea ice can be modeled in spatial coordinates by a momentum balance equation where the internal and external forces are equated to the material time derivative of the momentum. Because the horizontal extent of the ice is much greater than its vertical extent, a two-dimensional momentum balance equation is generally solved with an ice thickness parameter, h, included to model the vertical dimension. In general, the ice thickness varies due to both dynamic and thermodynamic effects. However, for this work the variation of h is neglected. The two-dimensional momentum balance equation in Cartesian coordinates is (Hibler, 1979; Gray and Morland, 1994; Schulkes et al., 1998)

$$(\rho h)\frac{D\mathbf{v}}{Dt} = \mathbf{t}_a + \mathbf{t}_w + \nabla \cdot (\boldsymbol{\sigma} h). \tag{1}$$

The ice velocity is $\mathbf{v}$, ρ is the ice density, h is the ice thickness, $\mathbf{t}_a$ is the air drag, $\mathbf{t}_w$ is the water drag, $\boldsymbol{\sigma}$ is the Cauchy stress tensor, and D/Dt indicates the material time derivative. The studies in this paper neglect the Coriolis force and sea-surface tilt.

The air drag is modeled as a quadratic function of the geostrophic wind velocity $\mathbf{v}_a$ with drag coefficient c_a, air density ρ_a and air turning angle α,

$$\mathbf{t}_a = c_a \rho_a \|\mathbf{v}_a\| R_a \mathbf{v}_a \tag{2}$$

with

$$R_a = \begin{bmatrix} \cos\alpha & -\sin\alpha \\ \sin\alpha & \cos\alpha \end{bmatrix}. \tag{3}$$

Following Schulkes et al. (1998), the water drag is a linear function of the difference between the ocean velocity $\mathbf{v_w}$ and the ice velocity $\mathbf{v}$ with drag coefficient c_w and water density ρ_w

$$\mathbf{t}_w = c_w \rho_w (\mathbf{v} - \mathbf{v}_w). \tag{4}$$

Quadratic drag laws have also been used. Numerical results for the problem under consideration are not sensitive to the exact form of the drag law.

The stress, $\boldsymbol{\sigma}$, is determined from the constitutive model, which in our case is an elastic-decohesive model. This model is discussed next.

ELASTIC-DECOHESIVE MODEL

In the pack ice, the horizontal extent of the ice is much larger than the vertical thickness. Thus, we will treat the pack ice with a two-dimensional, plane stress model. Within this model, fracture is assumed to occur orthogonal to the plane of the ice. The basic idea is that the ice is modeled as an isotropic, elastic solid until failure begins. Failure begins when some measure of the traction on a failure surface reaches a critical value. During decohesive failure, the traction on the failure surface is reduced from non-zero to zero. At complete separation, there is no traction on the new free surface, however, other stress components can still be nonzero. There are three aspects of the model that need to be examined, (1) the criterion to initiate failure, (2) the determination of the failure direction (*i.e.*, orientation of the crack or lead), and (3) the mechanism for traction reduction. These aspects are discussed briefly below. Full details regarding the model can be found in Schreyer et al. (2006).

Given the current stress at a material point, $\boldsymbol{\sigma}$, the criterion to initiate failure is expressed by a failure function $F(\boldsymbol{\sigma})$. The elastic region in stress space is given by the condition $F < 0$. Failure occurs when $F = 0$ and $F > 0$ is not allowed. This failure function is similar to a yield function in plasticity theory. Figure 3 shows an example of the failure function for the decohesion model used in this work. Specifically, the stress at which failure occurs is the envelope in stress space defined by $F(\boldsymbol{\sigma}) = \max_n F_n(\boldsymbol{\sigma}, \mathbf{n})$, where $F_n(\boldsymbol{\sigma}, \mathbf{n})$ is the failure function for a crack oriented with a normal to its surface given by $\mathbf{n}$. Thus, the orientation of the lead is determined as the $\mathbf{n}$ that maximizes F. The search for the correct orientation is done analytically or numerically, depending on the specific form for F_n (Schreyer et al., 2006).

Let $\mathbf{t}$ be a vector tangent to the lead so that $\mathbf{n}$ and $\mathbf{t}$ form a right-handed coordinate system. The functional form of F_n is expressed in terms of the normal and tangential components of the traction on the failure surface, $\tau_n = \mathbf{n}\cdot\boldsymbol{\sigma}\cdot\mathbf{n}$ and $\tau_t = \mathbf{t}\cdot\boldsymbol{\sigma}\cdot\mathbf{n}$, and the tangential stress, $\sigma_{tt} = \mathbf{t}\cdot\boldsymbol{\sigma}\cdot\mathbf{t}$. The function F_n combines a brittle decohesion function with a ductile failure function to allow for multiple modes of failure including mixed modes (Schulson, 2004). The brittle decohesion function is defined as

$$B_n = \frac{\tau_n}{\tau_{nf}} - f_n\left(1 - \frac{\langle -\sigma_{tt}\rangle^2}{f_c'^2}\right) \tag{5}$$

where τ_{nf} is the tensile failure stress, and f_c' is the failure stress in uniaxial compression. The McCauley bracket, $\langle\cdot\rangle$ indicates that the tangential stress term only appears when σ_{tt} is negative.

The softening parameter, f_n, is a function of the normal component of the jump in displacement, u_n and has a value of one at the initiation of decohesion and decreases to zero as the lead opens. Specifically, $f_n = \langle 1 - u_n/u_0\rangle$. The lead is fully opened when u_n, reaches a predetermined value, u_0. This softening parameter forces the normal component of the traction on the crack surface to reduce to zero as the crack opens (*i.e.*, as u_n increases). As f_n decreases, B_n also goes to zero. We will see below that B_n going to zero forces the tangential component of traction on the failure surface to zero also. Thus when the crack is fully open,

there is no traction on the surface. In this manner, the parameter f_n accounts for the reduction of traction as decohesion proceeds.

If B_n is used to indicate the failure stress, and σ_{tt} is zero, then failure initiates when the normal component of traction, τ_n reaches the value τ_{nf}, since $f_n = 1$ at the initiation of failure. This scenario represents failure under pure tension. The normal to the crack would be in the direction of maximum principal stress. This is a classical criterion that is often used in fracture mechanics for brittle failure. The presence of σ_{tt} in the brittle failure criterion has been included to allow for the possibility of axial splitting (Schulson, 2004; Schreyer et al., 2006). This term potentially reduces the critical value of the normal traction when σ_{tt} is compressive.

The final form of F_n incorporates B_n along with a term including the tangential component of traction

$$F_n = \left(\frac{\tau_t}{s_m \tau_{sf}}\right)^2 + e^{\kappa B_n} - 1. \tag{6}$$

In this expression, τ_{sf} is the failure stress in shear. The shear magnification factor, s_m, magnifies τ_{sf} when the ice is under compression. In pure shear, the only nonzero term in F_n is the tangential component of traction, τ_t. By the definition of τ_{sf} and f_n, failure initiates when $\tau_t = \tau_{sf}$ and $f_n = 1$, giving the relation $s_m^2(1 - e^{-\kappa}) = 1$ to define the parameter κ.

When the ice is being compressed, the brittle failure criterion is negative, $B_n < 0$. Thus, under large compression, the exponential term in the expression for F_n is small. If the exponential term were absent, failure would occur when τ_t reaches the shear failure strength $\tau_{sm} = s_m \tau_{sf}$. This is a Tresca-like criterion that is often used in failure mechanics as a model for shear failure. Under pure shear, the failure surface is oriented at $\pm 45^\circ$ to the direction of maximum principal stress. The brittle and shear failure criteria in the expression for F_n are combined to give a smooth transition from one mode to the other as the stress state varies. The orientation of the lead with respect to the direction of maximum principal stress also varies smoothly, as observed experimentally (Schulson, 2004).

The elastic-decohesive constitutive model is implemented similarly to an elastic-plastic constitutive model (Schreyer et al., 2006). The ice behaves elastically until the stress reaches a point where failure occurs. Once decohesion is initiated a lead is formed with a jump in displacement, $[\mathbf{u}]$, and an associated direction defined by a vector normal to the lead, $\mathbf{n}$. A decohesion strain is calculated by regularizing the jump in displacement,

$$\mathbf{e}^d = \frac{1}{L}([\mathbf{u}] \otimes \mathbf{n}) \tag{7}$$

where the length scale, L, is determined so to dissipate the correct energy (Schreyer et al., 2006). The elastic strain is then calculated as the difference between the total strain and the decohesive strain, $\mathbf{e}^e = \mathbf{e} - \mathbf{e}^d$. The stress is then

$$\boldsymbol{\sigma} = \mathbb{E}\mathbf{e}^e \tag{8}$$

where $\mathbb{E}$ is a fourth order elasticity tensor. For the ice calculations, the material is assumed to be isotropic. Therefore $\mathbb{E}$ contains only two parameters: the bulk modulus, B, and the shear modulus G.

The numerical implementation of the constitutive model follows a standard approach in computational mechanics. In outline, the numerical algorithm to enforce decohesion proceeds as follows. Given the current stress $\boldsymbol{\sigma}$ and an increment in the strain, $\Delta\mathbf{e}$, at a material point:

1. Compute an elastic trial stress, $\boldsymbol{\sigma}^{\text{trial}} = \boldsymbol{\sigma} + \mathbb{E} : \Delta\mathbf{e}$.
2. Find the direction of failure if none existed previously, or check for a new direction.
3. For each failure direction, find $[\mathbf{u}]$ to bring $F > 0$ back to $F = 0$.

After failure is initiated for some direction, the components of $[\mathbf{u}]$ evolve according to a normal flow rule, as shown below.

$$\begin{aligned} \dot{u}_n &= \dot{\omega}\frac{\partial F}{\partial \tau_n} \\ \dot{u}_t &= \dot{\omega}\frac{\partial F}{\partial \tau_t} \end{aligned} \tag{9}$$

where $\dot{\omega}$ is the evolution parameter. These equations are used along with the consistency condition $\dot{F} = 0$ to find the jump in displacement. A secant method is used to solve these nonlinear equations.

When u_n is equal to u_0, the lead is fully open and the traction on the surface is zero. At this point the above evolution equations are no longer used. Instead, if the trial stress gives a positive normal component of traction then the jump in displacement will continue to open. The amount of opening is determined to make the traction zero (the free surface condition). If the load reverses so that the lead closes, it might be possible to obtain a negative normal component of traction. In this case the tangential component of the displacement jump is adjusted, if necessary, to keep $F_n \leq 0$. These operations provide a simple closing model for leads. More sophisticated models that include ridging forces and/or sliding friction are possible, but beyond the scope of this work.

THE MATERIAL-POINT METHOD

MPM partitions the ice into material elements that are followed in a Lagrangian sense throughout the computation. Each material point has a mass, position, velocity and stress, as well as material parameters and internal variables needed for the constitutive model. Each point carries material properties without incurring the numerical diffusion associated with Eulerian advection schemes. However, computing gradients of field quantities based on the material-point description is complicated since neighbors of a given point can change during a simulation. In order to keep the computational work linear in the number of material points, a second discretization is used for solving the momentum equation. This representation of the solution is a background computational mesh that covers the domain. For the simulations discussed in the next section, a regular square mesh is used. In outline, the steps of the MPM computational cycle are:

1. In the first step of the computational cycle, information carried by the material points is projected on to the background mesh to determine the mass and velocity on the mesh. Internal forces at the nodes of the background mesh are determined directly from the material-point stress using a gradient weight and the material-point volume.

2. External forces on the nodes of the background mesh, for example due to wind or ocean drag, Coriolis or tilt forces, are added to the internal forces (the stress divergence), and the momentum equation is solved on the background mesh. During this Lagrangian phase of the calculation, each element is assumed to deform in the flow of material so that points in the interior of the element move in proportion to the motion of the nodes. That is, given the velocity at the nodes, element shape functions are used to map the nodal velocity continuously to the interior of the element.

3. The mesh solution in the last step is used to update the state of each material point. The positions of the material points are updated by moving them in the single-valued, continuous velocity field that arises from the mapping through element shape functions. The velocity is updated similarly. In its simplest form, strain increments are obtained from gradients of the nodal velocities on the background mesh, evaluated at the material point positions. Then, given a strain increment at a material point, constitutive routines are used to update the stress.

4. The material points now carry all information about the solution; therefore, one can choose whether to continue the calculation in the Lagrangian frame or map information from the material points to another grid. In this work, the same fixed Eulerian grid is used throughout the calculation.

Details regarding MPM and its implementation for sea ice dynamics can be found in Sulsky et al. (2005).

CALCULATIONS

Schulkes et al. (1998) identify a simple test problem that seems to distinguish properties of various ice rheologies. In that work, a simple rectangular region of ice is subjected to wind forcing and ocean drag. Two adjacent boundaries of the rectangle represent free surfaces and the other two boundaries represent shorelines. Along the shore, the ice has no normal component of velocity but is allowed to slip freely, relative to the shore, in the tangential direction. For the MPM calculation, a 25 km by 50 km region of ice is placed so that the left and bottom ice boundaries coincide with the left and bottom background-grid boundaries. The left and bottom grid boundaries are identified with the straight shoreline. The ice is initially at rest and has a thickness of 2 meters. A plot of the grid and ice region is shown in Figure 1. The background grid has 2.5 km square elements The ice is discretized using four material points per element.

A constant surface wind velocity is applied; and it is assumed that the ocean velocity is zero. Thus, the ocean drag is just proportional to the ice velocity. Parameters used for all calculations are shown in Table 1. Parameters for the decohesion model are given in Table 2 for the first calculation. These decohesion parameters are chosen to match experimental data and from kinematic studies (Schreyer et al., 2006).

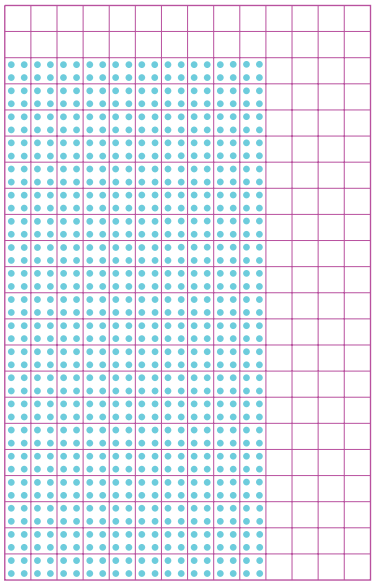

Figure 1: The ice is a 25 km by 50 km region discretized using 4 material points per element. The background grid consists of 2.5 km square elements.

Table 1: Common Parameters Used for All Calculations

ice density	ρ	917 kg m^{-3}
ice thickness	h	2 m
air density	ρ_a	1.20 kg m^{-3}
air drag coefficient	c_a	0.0012
air turning angle	α	0
sea water density	ρ_w	1026 kg m^{-3}
sea water drag coeff	c_w	0.00536
sea turning angle	β	0
shear modulus	G	3.6765×10^5
bulk modulus	B	11.905×10^5

In the first calculation a geostrophic wind velocity of -5.98 m/s in the y-direction is used in order to match the wind stress of 0.05 kg m^{-1}s^{-2} used in Schulkes et al. (1998). The time stepping is explicit, with the time step controlled by the CFL condition based on the elastic wave speed and the background mesh size. The time step is about $\Delta t = 30$ secs, requiring about 7800 steps for a total simulation time of three days. It is worth noting that this time step is about four orders of magnitude larger than the time step that would be required for a stable, explicit viscous-plastic simulation with the same mesh size (Sulsky et al., 2005).

Table 2: Decohesion Parameters Used for Calculation 1

τ_{nf}	15.0 KPa
τ_{sf}	9.0 KPa
u_0	100 m
s_m	4
κ	0.064538521
f_c'	75 KPa

In this calculation the ice did not deform significantly over the three days. The maximum stress in the ice is not sufficient to initiate decohesion and the ice response to forcing is purely elastic. After a brief transient period, the motion is quasistatic and the momentum balance is primarily a balance of the wind stress and the internal forces. An approximate solution is obtained by assuming the ice velocity is zero and the only nonzero Cauchy stress component is the yy-component, σ_{yy}. In order to balance the wind stress, σ_{yy} is linear in y, zero at the top of the ice and -1250 Pa at the bottom. The two-dimensional simulation with slip boundary conditions shows this general behavior with an approximately linear stress profile along the y-direction, as shown in Figure 2.

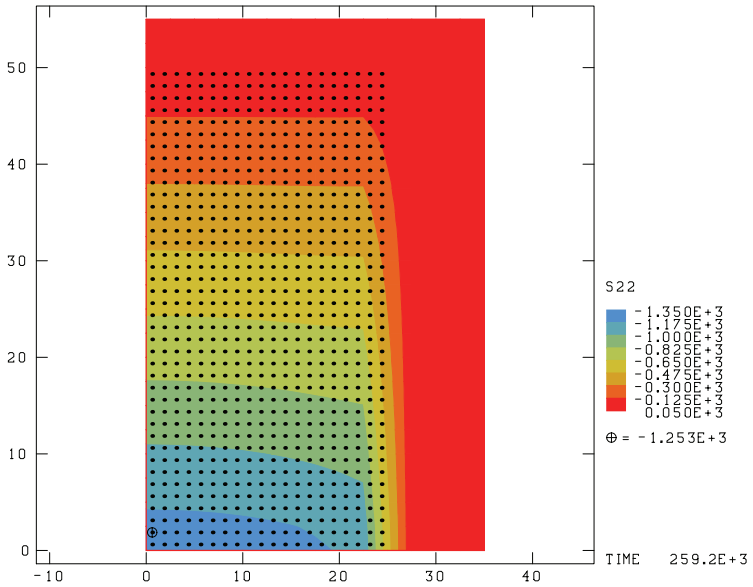

Figure 2: Contour plot of the yy-component of the Cauchy stress for calculation 1.

The calculations in Schulkes et al. (1998) use viscous and viscous-plastic constitutive models which tend to show more flow than the elastic model used above. One example is a viscous-plastic model similar to the one developed by Hibler (1979). This model is based on an elliptic yield curve, the size of which is determined by an ice strength. The ice strength in units of force per unit length is given by

$$P = P^* hA \exp(-K(1-A)) \tag{10}$$

Table 3: Parameters Used for Calculation 2

τ_{nf}	300 Pa
τ_{sf}	180 Pa
u_0	100 m
s_m	4
κ	0.064538521
f_c'	1500 Pa

where A is the ice compactness, h is the ice thickness, P^* is a constant taken to be 5×10^3 kg m^{-1}s^{-2}, and K is a constant equal to 15. In Schulkes et al. (1998), the initial compactness is 0.9. The uniaxial compressive strength, per unit thickness, based on this elliptical yield surface is

$$\frac{2P^* \exp(-K(1-A))}{1+e^2}. \tag{11}$$

For the parameters cited above, and with an eccentricity $e = 2$, the uniaxial compressive strength is about 450 Pa. Figure 3 shows a plot of this elliptical yield surface, per unit thickness, plotted in principal stress space.

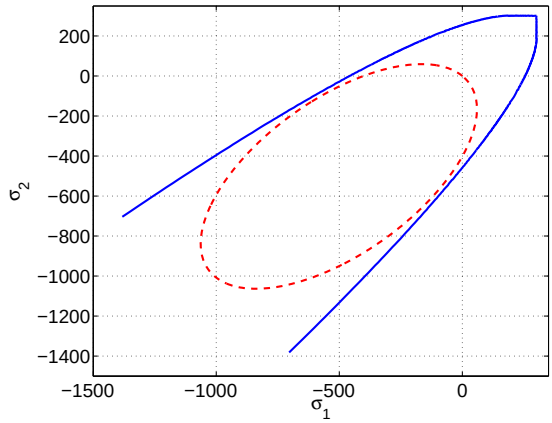

Figure 3: The dashed line is a viscous-plastic yield surface and the solid line is a decohesive failure surface. The axes show the values of principal stresses.

In the next MPM calculation, the parameters defining the failure function are reduced to more closely match the viscous-plastic yield surface to the decohesion surface. Specifically, τ_{nf} is reduced to 300 Pa. The other parameters keep the same proportion as in the first calculation. The values are listed in Table 3. Figure 3 compares the decohesive failure function and the yield function associated with the viscous-plastic model. To better resolve the large deformation, the background grid is reduced to a 1.25 km square mesh. The calculation is explicit in time, with the time step determined by the CFL condition, as before. Due to the finer mesh, the time step is about $\Delta t = 15$ seconds and the full simulation requires roughly 16000 steps for the full three days.

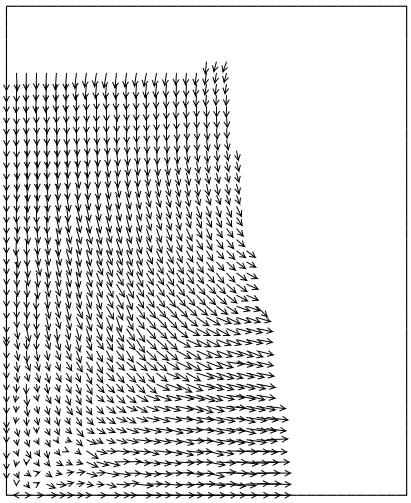

(a)

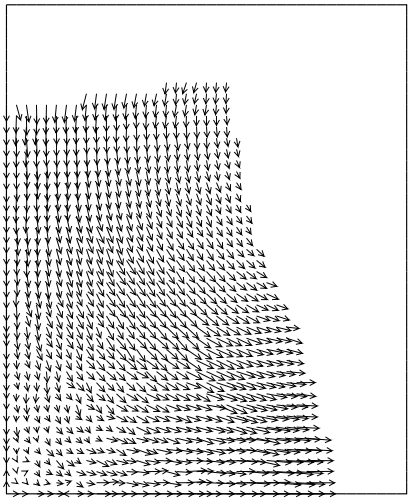

(b)

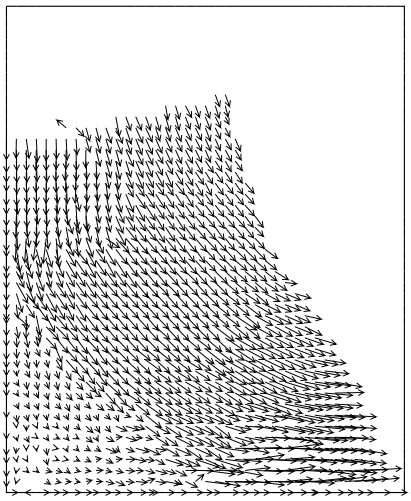

(c)

Figure 4: Ice velocity after (a) 1 day, (b) 2 days, and (c) 3 days for calculation 2.

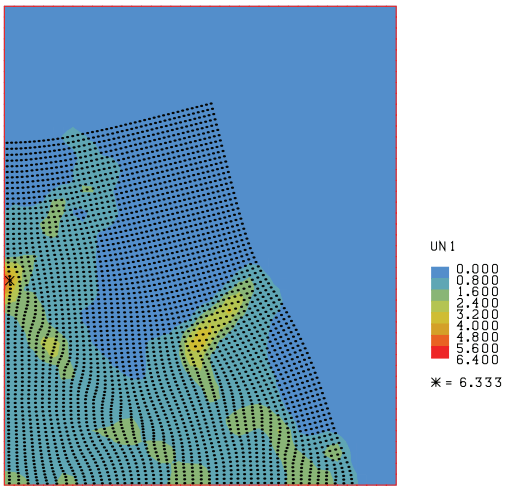

(a)

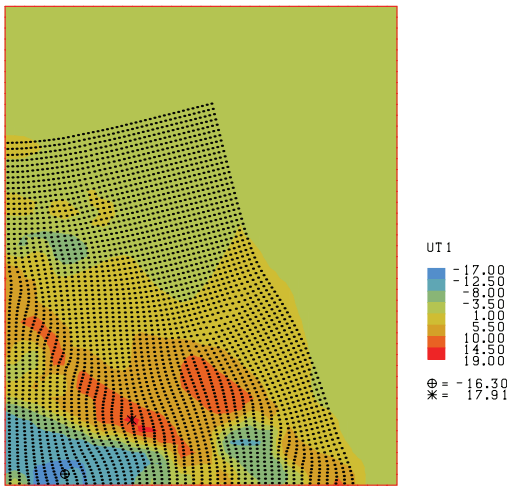

(b)

Figure 5: Contour plot of the (a) normal and (b) tangential components of the displacement jump after 3 days.

Figures 4(a)-(c) show the velocity vectors after one, two and three days, respectively, for this second calculation. The ice is driven toward the solid boundary at the bottom of the domain. At this bottom boundary there is considerable deformation of the ice as the free surface moves out to the right. The velocity is smaller in the lower left corner of the domain than elsewhere. The region of lower velocity is separated from the main flow by a zone of high shear. Figures 5(a)-(b) show contour plots of the normal and tangential components of the displacement jump, respectively. These components are scaled by $u_0 = 100$ m. Thus, the largest normal opening is about 600 m and occurs near the left side of the domain. There is also a similarly large opening along a crack roughly normal to the right side of the ice sheet. The tangential component of the displacement jump has a larger maximum magnitude, almost 2 km. It is apparent that the shear zone seen in the velocity field corresponds to a lead where there is a large tangential displacement between the sides of the lead. Thus, two main leads appear in the simulation. The first lead opens and is accompanied by relatively large shear, and the second lead mainly opens with relatively little shear. Overall the deformation bears some similarity to the deformation presented in Schulkes et al. (1998) using the viscous-plastic model where a similar shear zone appears. However, the opening of the second lead does not seem to correspond to any feature of the viscous-plastic simulation.

DISCUSSION

The first calculation where the ice sheet remains elastic provides a simple test of the numerical method since an approximate analytical solution can be used for comparison. The values of τ_{nf}, τ_{sf} and f_c' used in this first calculation did not result in significant deformation under the prescribed wind stress. Experiments and kinematic studies (Schreyer et al., 2006) indicate that the parameters used in this simulation are characteristic of an intact ice sheet. In contrast, there is significantly more deformation seen in computations with a viscous-plastic model shown in Schulkes et al. (1998). As discussed above, the initial compactness of 0.9 used in those simulations implies that the ice sheet is not intact, but contains 10% open water. The presence of water reduces the strength of the intact ice sheet. Note that this reduction occurs uniformly and isotropically throughout the domain.

The second calculation, where the decohesion parameters are reduced, is an isotropic approximation to the case where the ice has multiple leads throughout that reduce its strength. This is analogous to having a low strength and a compactness less than one for the viscous-plastic model. Under these conditions the extent of the deformation using the elastic-decohesive model is similar to that observed using a viscous-plastic model. Using the elastic-decohesive model, the deformation is seen to result from the formation of two principal leads. One lead opens and shears while the failure mode for the second lead is primarily an opening mode. This simulation provides an example of the information that is available through the decohesion model. It should be noted that once decohesion initiates the ice is no longer an isotropic material. The traction on the surface of a lead goes to zero as it opens, but components of stress orthogonal to the lead can be nonzero. Although not done in this paper, the area associated with the open lead can be calculated. Future studies can add thermodynamic effects that would allow the exposed water to freeze and grow new ice. Standard methods that track ice thickness distributions can also be added to give a more complete model of the ice sheet.

Instead of uniformly reducing the strength of the ice sheet when water is present, it is possible, using the elastic-decohesive model, to initialize water concentrated in leads that would provide directional weaknesses at various locations. The ice would have material parameters associated with intact ice, as used in the first calculation. Using this approach, the weakness in the ice would no longer be isotropic and the response to wind loading would depend on the orientation of the pre-existing leads. One can imagine two simple cases. In the first case, pre-existing leads are oriented parallel to the wind velocity, and in the second case pre-existing leads are oriented perpendicular to the wind velocity. In the first case, the parallel leads would not evolve under the loading and the ice would have a purely elastic response as in calculation 1. There would be rather little deformation. In the second case, the loading would initially result in the leads closing, but once the leads closed an elastic response similar to that shown in calculation 1 would occur and any significant deformation of the ice would be due to the closing leads. These deformation modes are difficult, if not impossible, to mimic with a viscous-plastic model.

CONCLUSIONS

We have presented a new, elastic-decohesive constitutive model for pack ice, and a numerical method, MPM, capable of treating displacement discontinuities as they form when leads appear. The constitutive model treats the ice as an isotropic, elastic solid for small stress. Under sufficient loading, the stress reaches a failure limit and a lead forms. The model parameters can be adjusted to provide the correct stress level at which failure should occur, and additionally, the proper orientation of the predicted leads. The latter feature is not usually considered in the literature, and therefore, is a unique feature of the model under consideration.

A simulation suggested by Schulkes et al. (1998) allows comparison of various ice rheologies. The presence of the free boundary on half of the domain, combined with slip conditions along the solid boundary on the other half of the domain, allows the ice to deform readily under loading. The resulting deformation also tests the capability of the numerical scheme. It is seen that MPM can handle large deformations since the background computational mesh is not used to represent the complicated geometry. Instead, a set of unconnected material points distort and flow through the background computational mesh. Information from the material points is projected onto the background mesh, where the momentum equation is solved. The mesh solution is then used to move the material points and to update their properties. The sample calculations demonstrate that an elastic-decohesive constitutive model can be used with the

material-point method to model sea ice dynamics. Whether this rheology accurately represents the behavior of sea ice is still an open question. The answer to this question can only come from additional numerical tests and comparison with observations.

ACKNOWLEDGMENTS

This material is based upon work partially supported by the National Science Foundation (under Grant No. DMS-0222253), by the Minerals Management Service and the National Aeronautics and Space Administration (under contract NNH04 CC 45C) and the Office of Naval Research (under contract N000-14-04-M-0005) .

REFERENCES

Gray, J. and Morland, L. (1994). A two-dimensional model for the dynamics of sea ice. *Phil. Trans. R. Soc. Lond. A*, 347:219–290.

Hibler, W. D. (1979). A dynamic thermodynamic sea ice model. *Journal of Physical Oceanography*, 9:815–845.

Schreyer, H., Monday, L., Sulsky, D., Coon, M., and Kwok, R. (2006). Elastic-decohesive constitutive model for sea ice. *Journal of Geophysical Research*, to appear.

Schulkes, R. M. S. M., Morland, L. W., and Staroszczyk, R. (1998). A finite element treatment of sea ice dynamics for different ice rheologies. *International Journal for Numerical and Analytical Methods in Geomechanics*, 22:153–174.

Schulson, E. M. (2004). Compressive shear faults within Arctic sea ice: Fracture on scales large and small. *Journal of Geophysical Research-Oceans*, 109.

Sulsky, D., Schreyer, H., Peterson, K., Kwok, R., and Coon, M. (2005). Using the material-point method to model sea ice dynamics. *Journal of Geophysical Research*, submitted.

Sulsky, D., Zhou, S.-J., and Schreyer, H. L. (1995). Application of a particle-in-cell method to solid mechanics. *Comput. Phys. Commun.*, 87:236–252.